# STUDY OF ELECTROCHEMICAL BEHAVIOR AND SMOOTHING OF ADVANCED ALLOY TI6AL4V WITH ULTRASONIC WAVES

Andrei Gheorghe [1], Dana Lepădatu[2], Daniel Ghiculescu [3] and Alexandra Banu [4]
[1] Polytechnic University of Bucharest, andygheo1995@gmail.com,
[2]Polytechnic University of Bucharest, lepadatudana96@gmail.com,
[3]Polytechnic University of Bucharest, daniel.ghiculescu@gmail.com,
[4]Polytechnic University of Bucharest, alexandrabanu14@yahoo.com

ABSTRACT: This research deals with the electrochemical behavior of the advanced material Ti6Al4V in 5% NaCl electrolyte solution as well as the smoothing of the semi-finished front surface by the ultrasonic cyclic stress-inducing effect on the microgeometry peaks. Laboratory experiments were carried out on the estimation of electrochemical parameters in relation to the studied material. The smoothing of the front surface was made by varying the distance between it and the end of the ultrasonic chain and also the energy consumption on the ultrasonic chain. Computerized models were developed using the finite element method of the material removal mechanism using ultrasounds, aiming to explain the specific phenomena of ultrasonic cavity in electrolytic environment.
KEYWORDS: electrochemistry, ultrasound, Ti6Al4V alloys, roughness

## 1. INTRODUCTION

Ti6Al4V is an alpha-beta titanium alloy with high strength-to-weight ratio and very good corrosion resistance, which recommend it for applications in the aerospace industry and in biomechanical fields (implants and prostheses), the construction of parts and prototypes for racing cars, marine applications, chemical industry, and gas turbine construction. This alloy covers 50% of the global use of titanium [1], [2].

In the aerospace industry, this titanium alloy is used in the construction of bolts and rails, as well as engines, due to its high reliability. It is used for fan blades and casing, window frames, wings housing due to its relatively low operating temperature. [3] In the medical field, Ti6Al4V is used as a result of its exceptional biocompatibility in the design of prostheses and implants, especially when contact is made directly with tissue or bone, process called osteointegration, for example in the replacement of a vertebra in the spine, maxillofacial prosthesis, screws, wires, expandable rib cages, replacement of a finger or whole leg. It is also used for its corrosion resistance when it comes in contact with fluids inside the body. It is not ferromagnetic, and the patient can undergo a magnetic resonance imaging (MRI) examination. Doctors use Ti6Al4V utensils such as needles and micro needle holders, scissors, suture tools, cavity vein clamps, Lasik equipment for eye surgery, dental dilators, retractors, surgical tweezers. In the dental field, the alloy is used as a replacement for a missing tooth or completely reconstruct it by fusing the titanium bolt and the jaw, all made possible by its life-long strength and resistance. In the naval industry, this is used due to its very good corrosion resistance, as marine water has no effect on material quality [4]. Considering the high strength and hardness characteristics and the mechanical strength of the advanced alloy of Ti6Al4V, its processing using conventional procedures raises problems of particular difficulty. In this case, the approach to processing with nonconventional processes is much more appropriate especially in terms of surface complexity, precision and roughness. Electrochemical processing (anodic dissolution) associated with ultrasound may be a convenient solution for the processing of this material.

## 2. CURRENT STATE

### 2.1 Physico-chemical-mechanical properties of the Ti6Al4V alloy

The physico-chemical-mechanical properties of the Ti6Al4V alloy that justify applications in the most diverse fields, such as the aerospace, medicine, and naval industry, are presented in Tables 1-3 [5], [6].

**Table 1.** Physical characteristics

| | |
|---|---|
| Density | 4,43 |
| Coefficient of thermal expansion at 20 ° | 8,6 µ/m °C |
| Coefficient of thermal expansion at 250 ° | 9,2 µ/m °C |
| Coefficient of thermal expansion at 500 ° | 9,7 µ/m °C |
| Specific heat capacity | 0,5263 J/g °C |
| Thermal conductivity | 6,7 W/m °K |
| Melting point | 1604-1660°C |
| Solid state | 1604°C |
| Liquid state | 1660°C |

**Table 2.** Chemical characteristics

| Component | Composition (%) |
|---|---|
| Ti | 90 |
| Al | 6 |

| | |
|---|---|
| V | 4 |
| Fe | max 0,25 |
| O | max 0,2 |

**Table 3.** Mechanical characteristics

| | |
|---|---|
| Brinell hardness | 334 |
| Hard Rockwell | 36 |
| Hardness Vickers | 349 |
| Elasticity | 880-950 MPa |
| Elongation at break | 14 % |
| Reduce the section | 36 % |
| Modulus of longitudinal elasticity | 113,8 GPa |
| Compression strength | 970 MPa |
| Traction resistance | 1450 MPa |
| Poisson's ratio | 0,342 |
| Resistance to fatigue | 240-510 MPa |
| Breaking resistance | 950 MPa |
| Shear modulus | 44 GPa |
| Shear resistance | 550 MPa |

## 2.2 Experimental installation

To measure the effect of ultrasounds on surface passivation, corrosion, and roughness, an installation was constructed using an electrochemical cell, an ultrasonic source and a potentiostat, and its layout is shown in Figures 1-2.

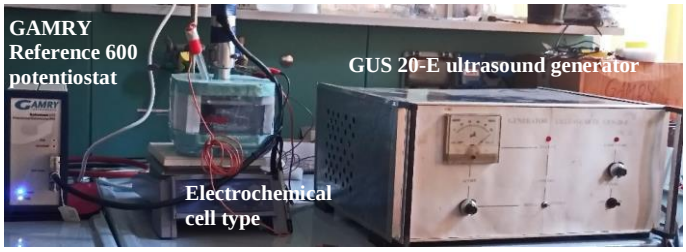


**Figure 1.** Composition of the experimental installation

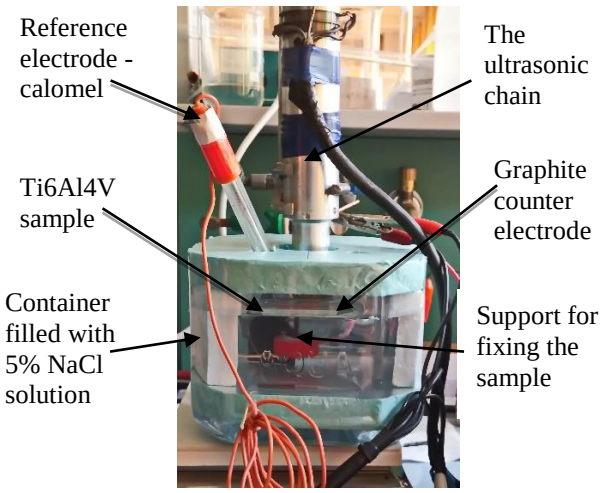


**Figure 2.** The electrochemical cell with ultrasonic aiding

## 2.3 Data on electrochemical processing of the Ti6Al4V alloy in the ultrasonic field

The influence of the ultrasonic field on the microgeometry of Ti6Al4V titanium alloy immersed in a 5% sodium chloride solution during (anodic dissolution) was studied, using different parameters.

Measurements were made at two values of the gap ($s_F$) between the end of the front surface of the ultrasonic chain and the piece of 10 mm and 2 mm, respectively, at two different powers, the step 10 and 6 of the ultrasonic generator, equivalent to about 100W and 60W, (consumption) of the ultrasonic chain.

Each sample was immersed for 60 minutes in said solution and subjected to an ultrasonic field in order to determine the influence of the power and the interstitial on the passivation of the surface, the surface and roughness of the workpiece. We measured the stationary potential with the Gamry Reference 600 to evaluate the ultrasonic effect. Figures 3-4 show the influence of ultrasonic chain drive power on passivation of the surface.

The general relation between the stationary potential and the passivation of the surface is explained by the fact that only *when the potential stationary increases the surface is passivated*. Figure 3 shows that sample 2 is passivated because the stationary potential increases up to 30 mV and then drops to -400 mV, equivalent to the situation when the surface is passivated and becomes constant at -380 mV, and for the other sample 1, the surface is passivated because the stationary potential decreases until it becomes constant at -420 mV. The analysis of the data from Figure 3 shows that at a higher power of the ultrasonic chain drive, the depassivation is stronger - ultrasounds have the ability to remove the passivated layer.

Figure 4 shows that the stationary potential of sample 3 is more stable than sample 4, and the surface is passivated because the potential increases to 25 mV, afterwards it decreases, being no longer passive and becomes constant at -400 mV. Sample 4 has an unstable surface because initially a phenomenon called the double-obscurative (load-unload) phenomenon occurs in the first 10 minutes, being more passive than the other sample because when the potential increases the sample is passivated. This pronounced increase occurs up to -150 mV, subsequently having small fluctuations around this value. It is notable that with the increase in the power of the ultrasonic chain, the depassivation is amplified. In conclusion, following the comparison of Figures 3 and 4, it is observed that when using low values of the gap between of the ultrasonic chain end and the part surface, and higher power of the ultrasonic chain, the depassivation effect of the surface is increased.

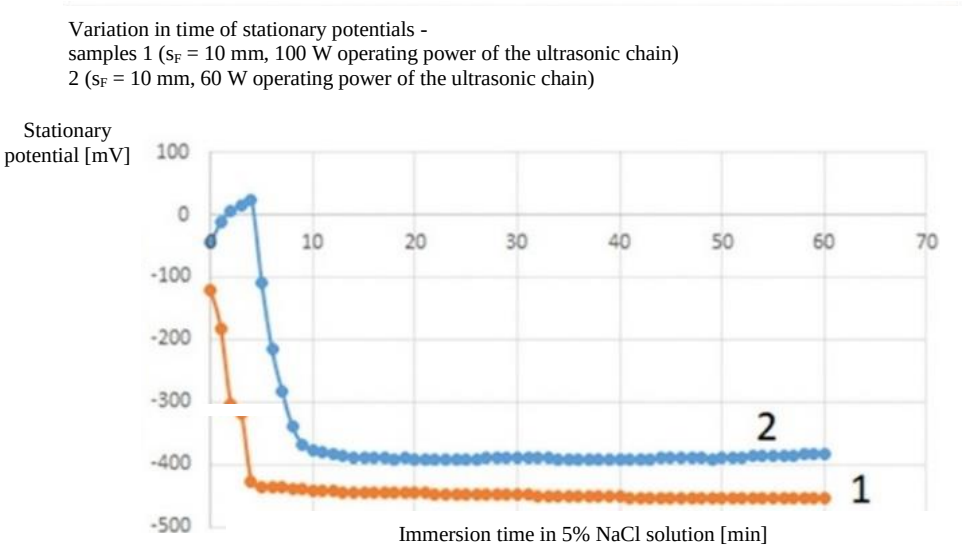


**Figure 3.** Variation of the stationary potential for 60 min in 5% NaCl solution for the ultrasonic-influenced Ti-Al-4V samples with 10 mm gap

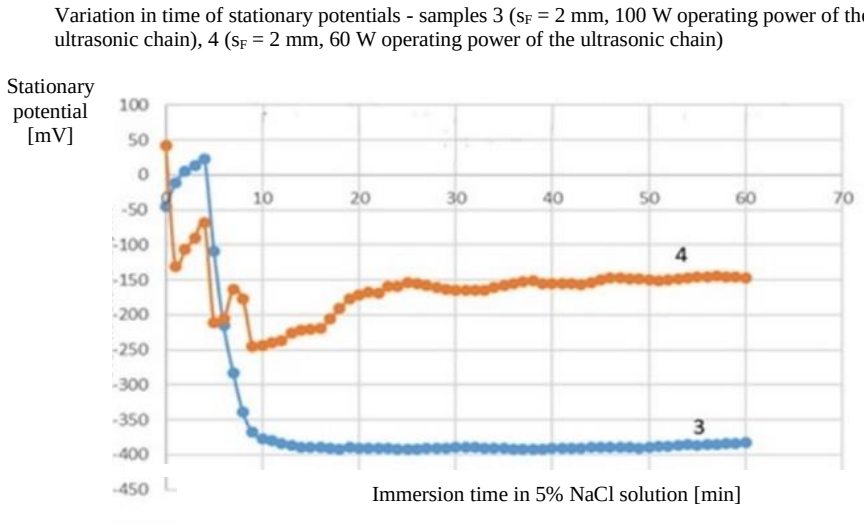


**Figure 4.** Variation of stationary potential for 60 min in 5% NaCl solution for ultrasonic-influenced Ti-Al-4V samples with 2 mm gap

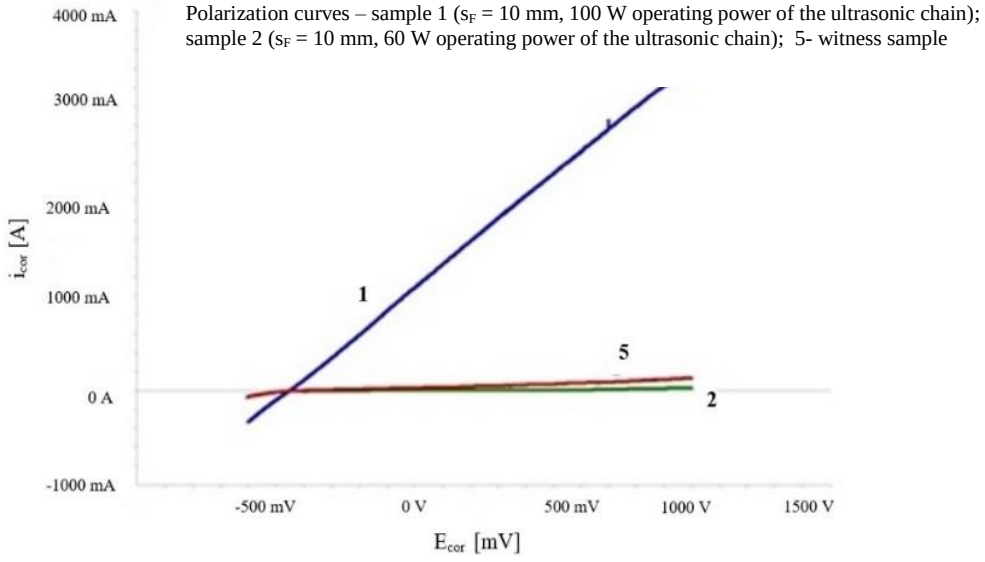


**Figure 5**. Anodic polarization curves of Ti-Al-4V titanium alloy samples with 10 mm gap

Polarization curves – samples 3 (sf = 2 mm, 100 W operating power of the ultrasonic chain);
4 (sf = 2 mm, 60 W operating power of the ultrasonic chain); 5- witness sample

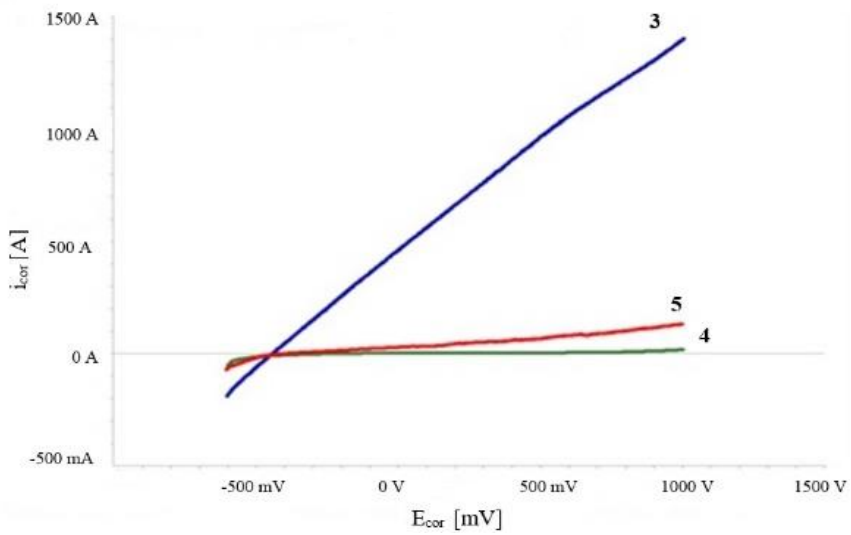


**Figure 6.** Anodic polarization curves of Ti-Al-4V titanium alloy samples with 2 mm gap

Figures 5-6 show the influence of the corrosion current on the corrosion potential to highlight the surface machinability. The general relationship between corrosion and surface corrosion is explained by the fact that only when corrosion increases, the passivation state is destroyed and the surface corrodes.
Figure 5 shows that sample 1 has a workable surface because when the corrosion current has a constant evolution, the surface corrodes by destroying the passivation state, reaching the value of 3200 mA, while sample 2 remains unprocessed because the corrosion current remains at around 0 A and does not destroy the passivation state of the surface. Figure 5 shows that when using a higher power of the ultrasonic bar, the sample is corroded more by looking at the increase of the $i_{cor}$ value.

**Table 4**. The values of the electrochemical parameters

| Name of the sample | Frontal gap, $s_f$ [mm] | The driving power of the ultrasonic chain [W] | Corrosion current, $i_{cor}$ [A] | Potential for corrosion, $E_{cor}$ [mV] | Speed of corrosion, $v_{cor}$ [mm/yr] |
|---|---|---|---|---|---|
| witness sample -5 | - | - | 2,63 | -406 | 0,04 |
| 1 | 10 | 100 | 13,10 | -451 | 3,85 |
| 2 | 10 | 60 | 6,25 | -395 | 0,22 |
| 3 | 2 | 100 | 224 | -451 | 2,97 |
| 4 | 2 | 60 | 3,17 | -221 | 0,05 |

In Figure 6, for sample 3, we note that there is a workable surface by destroying the passivation state as the corrosion current increases to 1450 A thus the sample surface is corroded, while sample 4 is not processed because the corrosion current remains constant at value 0 A.
Analyzing the data in Figure 6 we can reason that, when increasing the power consumed on the ultrasonic chain, but also the gap decrease at 2 mm, the volume of the removed material is increased, phenomenon indicated by the increase of the $i_{cor}$. Table 4 shows the values of the electrochemical parameters extracted from the polarization curves data.

## 2.4 Ultrasonic smoothing in the electrochemical field of the alloy surface of a Ti6Al4V

Table 5 shows the roughness measured by AFM at different values of the gap between ultrasonic chain and workpiece, and the various ultrasonic chain drive powers.

We note that when using 100 W ultrasonic chain drive power for both sample 1, where we had a 10 mm work gap, and sample 3 where the gap was 2 mm, the ultrasonic shock wave resulted from the development of the cavitation, then propagated perpendicularly to the surface of the piece, thus resulting an average arithmetic roughness of the measurements (Ra) of 68,64 nm and the mean root of the peaks and valleys (RMS) of 90,83 nm, and 133,5 nm and 164.9 nm respectively. Thus, a higher roughness was obtained than with the other two samples. When using 60 W ultrasonic chain drive power for sample 2, where a 10 mm work gap was used, as well as for sample 4, where the gap is 2 mm, the ultrasounds came parallel to the work surface and a surface roughness of 38.9 nm Ra and RMS of 50.17 nm, 40.16 nm and 51.9 nm respectively resulted.

In general, at power decrease on ultrasonic chain at 60 W, produced lower values of the samples roughness.

**Table 5.** The measurements obtained at atomic force microscopy

| Witness sample - 5 | $s_f$ = 10 mm | | $s_f$ = 2 mm | |
|---|---|---|---|---|
| | 100 W ultrasonic chain drive power | 60 W ultrasonic chain drive power | 100 W ultrasonic chain drive power | 60 W ultrasonic chain drive power |
| | 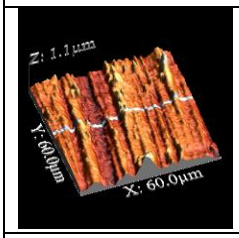 | 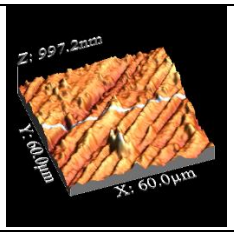 | 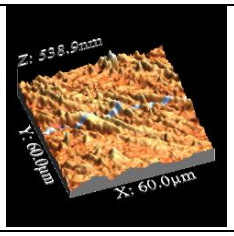 | 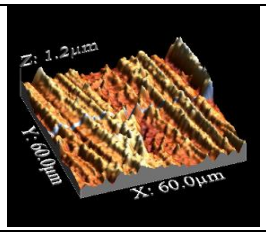 | 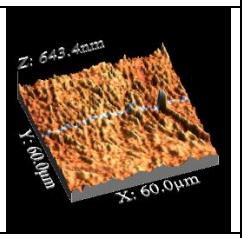 |
| | 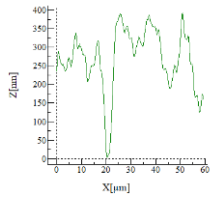 | 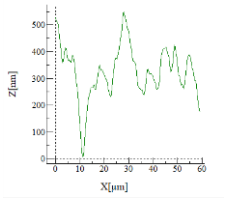 | 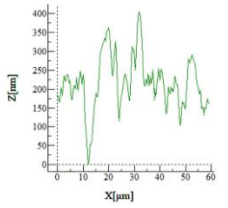 | 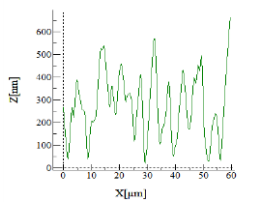 | 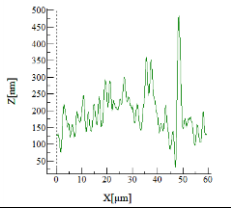 |
| RMS: 80,11 nm<br>Ra: 61,24 nm | RMS: 90,83 nm<br>Ra: 68,64 nm | RMS: 50,17 nm<br>Ra: 38,09 nm | RMS: 164,9 nm<br>Ra: 133,5 nm | RMS: 51,9 nm<br>Ra: 40,16 nm |

## 3. MODELING WITH FINITE ELEMENT METHOD OF MATERIAL REMOVAL

To perform the modelling of material removal by ultrasonic effect with high efficiency using Comsol Multiphysics, the first stage consists in parameterizing [8] the profile microgeometry of the sample (a), and the model its achievement (b), according to Figure 6.

a)

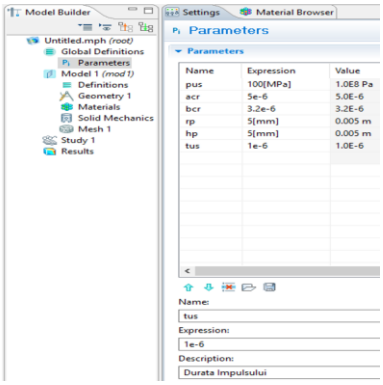

b)

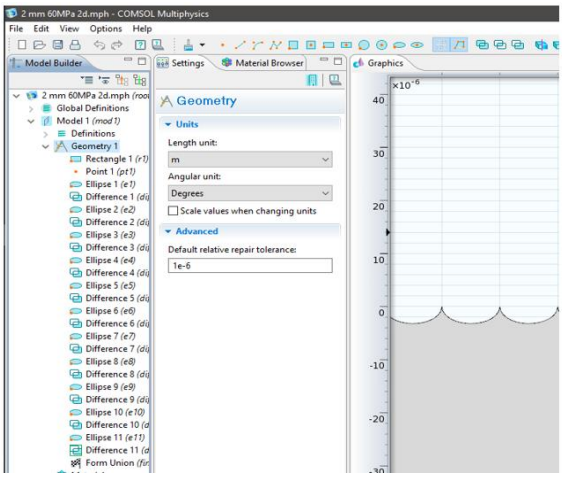

**Figure 6**. Model parameterization (a) and geometry achievement (b)

After the geometry is completed, the Ti6Al4V material is added to the program, and for the study of the effect of the ultrasonic pressure, the previously realized model is discretized, according to Figure 7.

a)

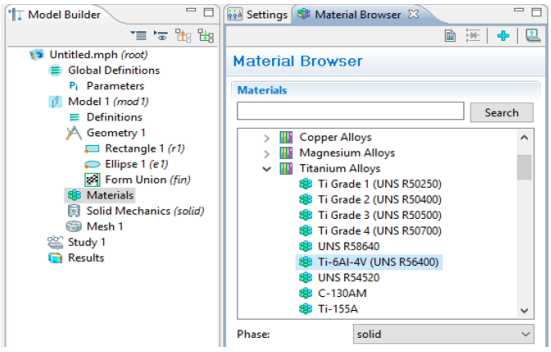

b)

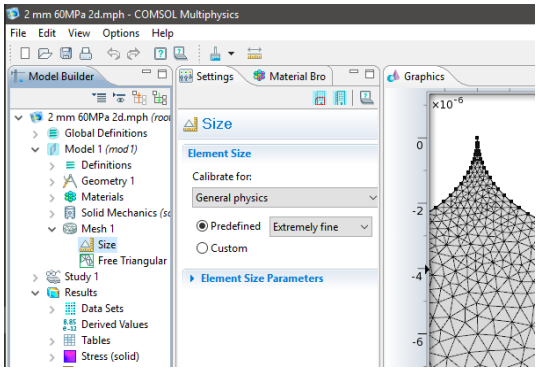

**Figure 7.** Adding the material to model (a), and model discretization (b)

The ultrasonic pressure was used as boundary load normal (*pus*, see fig. 6.a) on sample frontal surface at 10 mm gap, and parallel on it, on the microgeometry profile at 2 mm gap - Figure 8. Direction of shock waves propagation due to ultrasonic cavitation induced in the working gap depends on the gap dimension.

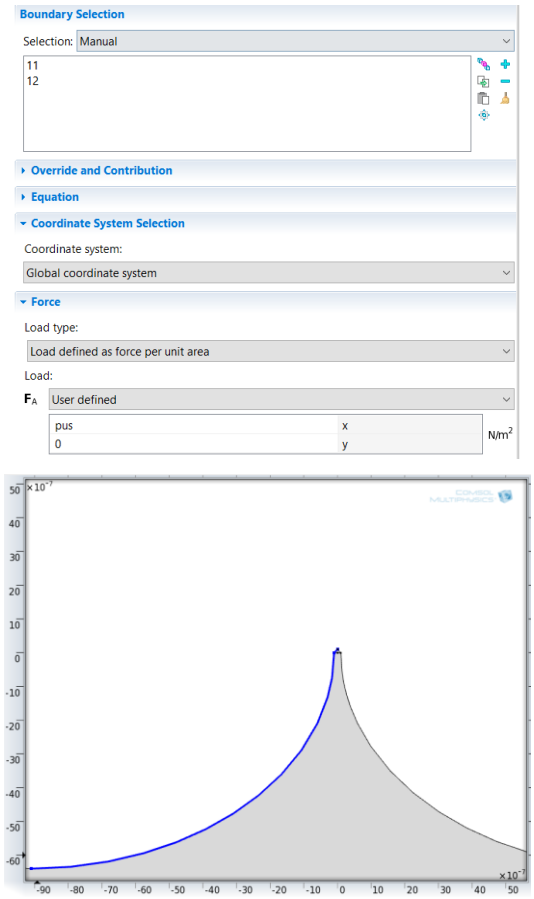


**Figure 8.** Boundary conditions as pressure load (pus) produced by ultrasonic cavitation

The Time Dependent menu was used, for the load applied during bubbles implosion (*tus*, see fig. 6.a) due to ultrasonic cavitation – Figure 9.

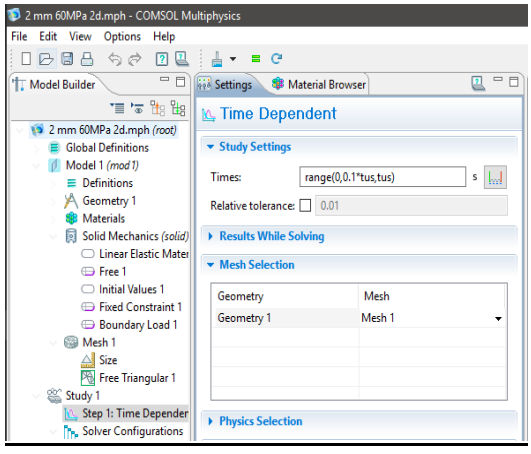


**Figure 9.** Establishing the time dependent parameter

In order to calculate the minimum value of unit effort at which the material breaks (is removed), we used the following formulas 1-2 [9]:

$$\tau_0 = 1.12(40 + 0,16\ \sigma_r) \quad (1)$$

$$\tau_{0t} = 1.5 * 0.6 * \tau_r \quad (2)$$

where, $\sigma_r$ is the breaking strength of the material and $\tau_r$ the shear resistance.

The calculated values are specified in the table 6.

**Table 6.** Shear and compression resistance

| $\tau_0$ [MPa] | $\tau_{0t}$ [MPa] |
|---|---|
| 218,62 | 727,5 |

Based on these ultimate values, corresponding to breaking of studied material, the removed material visualization by ultrasonic shock waves was setup – figure 10.

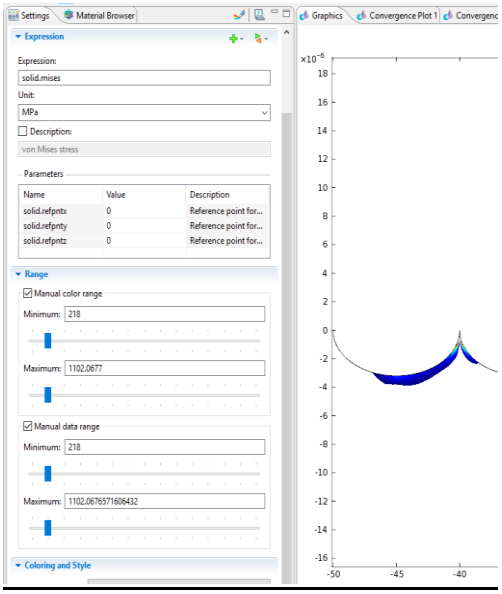


**Figure 10.** Setup for visualization of removed material due to ultrasonic cavitation effect

## 4. RESULTS

Table 7 presents the initial data used for finite elements modelling of material removal mechanism in terms of pressure exerted by ultrasonic cavitation.

**Table 7.** Variable key-parameter for material removal

| $s_F$ [mm] | Ultrasonic pressure, pus [MPa] | | | | |
|---|---|---|---|---|---|
| 10mm | 60 | 220 | 400 | 800 | 1000 |
| 2 mm | 60 | 80 | 100 | 120 | 140 |

As it can be seen in tables 8-9, when the pressure is applied perpendicularly and from longer distance (gap size $s_F$ =10 mm), the results appear, i.e. removed layer, at high ultrasonic pressures, over 400 MPa due to the compressive strength which is about 970 MPa. On the contrary, at lower distance (gap size $s_F$ =2 mm), the pressure is applied tangentially on the profile micro-geometry (surface roughness), which determines good productivity at low pressures, but at pressures greater than 60 MPa too much material is taken and thus, the surface roughness is increased. Under these assumptions resulted from finite element modelling of material removal, one can figure out that an optimization process is required depending on the process goal.

**Table 8. Results for the gap $s_F$ = 10 mm**

| Ultrasonic pressure [MPa] | Von Mises stress over ultimate strength [MPa] |
|---|---|
| 60 | 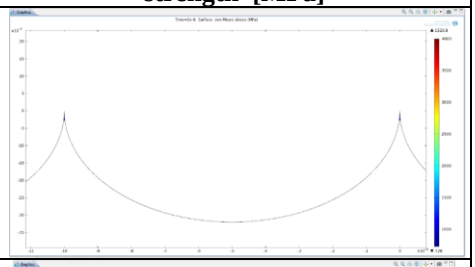 |
| 220 | 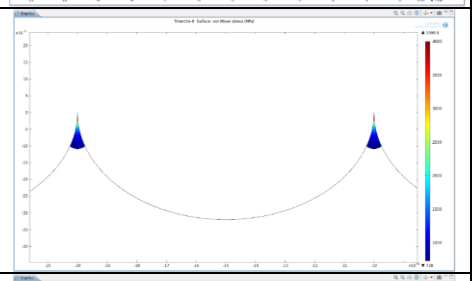 |
| 400 | 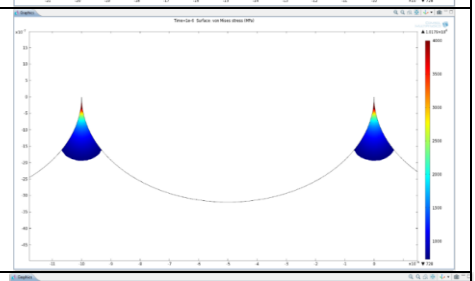 |
| 800 | 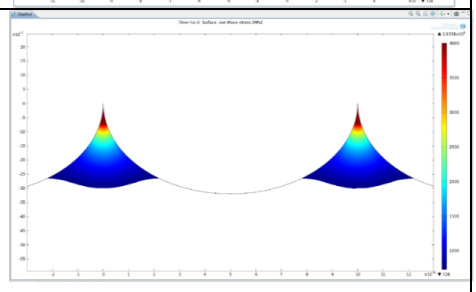 |
| 1000 | 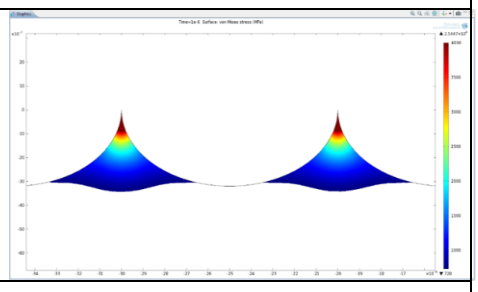 |

Using the date provided by finite element modeling of ultrasonic material removal mechanism, the depth variation of removed layer depending on applied pressure on sample microgeometry were presented in the two studied cases, related to gap size between ultrasonic chain end and sample frontal surface, subjected of ultrasonic cavitation – Figures 9 and 10.

**Table 9. Results for the gap $s_F$ = 2 mm**

| Ultrasonic pressure [MPa] | Von Mises stress over ultimate strength [MPa] |
|---|---|
| 60 | 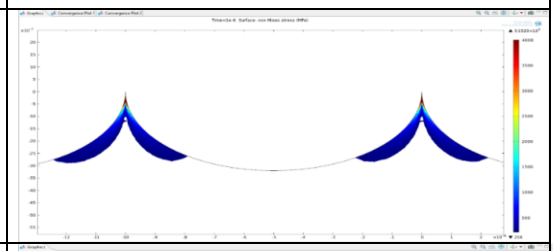 |
| 80 | 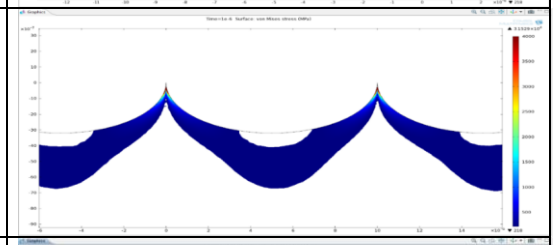 |
| 100 | 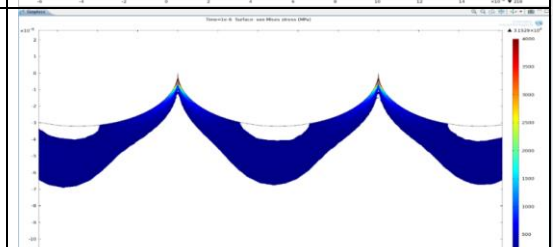 |
| 120 | 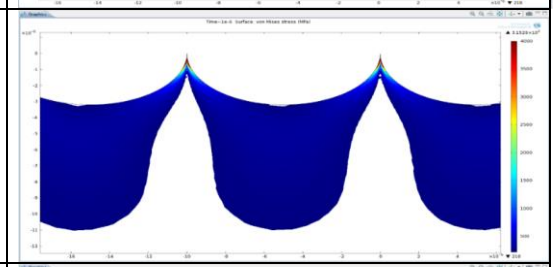 |
| 140 | 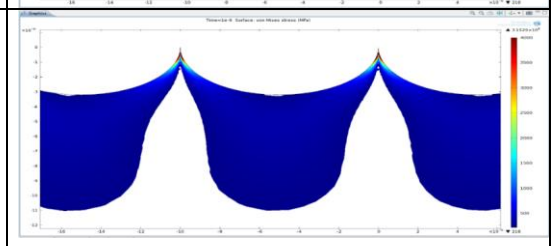 |

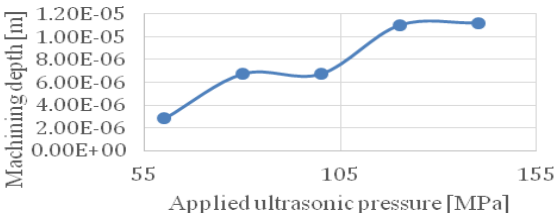


**Figure 9**. Depth variation of removed layer at gap of 10 mm

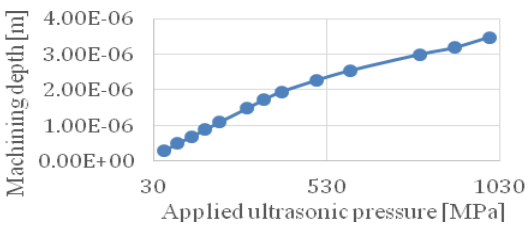


**Figure 10**. Depth variation of removed layer at gap of 2 mm

## 5. CONCLUSIONS

The description of the electrochemical behavior of the Ti6Al4V alloy based was achieved based on the experimental data obtained using the measurements by the potentiostat GAMRY Reference 600, supplying from GUS 20-E ultrasonic generator and using three electrodes: the reference-calomel electrode, the graphite counter electrode and the studied sample. Two main parameters were used for characterization of the ECM behavior: stationary potential ($E_{cor}$) and corrosion current ($i_{cor}$).

Evaluation of the surface microgeometry was studied using the roughness parameters RMS and Ra through the atomic force microscope (AFM).

Computerized modelling of the effect of ultrasonic cavitation on surface microgeometry was achieved, highlighting the volume of material removed through the effect on the roughness, and qualitative validation of the modelling results by AFM measurements.

Following the analysis of the electrochemical behavior it was found that:

The higher the power of the ultrasonic chain, the stronger the depassivation is achieved.

When using lower values of the frontal gap between ultrasonic chain end and sample surface, the passivation effect is increased.

Since the power consumed on the ultrasonic chain increases, the volume of material removed grows.

Regardless of the size of the frontal space, by introducing ultrasonic pressure, the volume of removed material increases, eliminating the passivated layer and the peaks of the surface microgeometry.

When increasing the working gap to relatively high values, the propagation of ultrasonic shock waves increases the roughness of frontal surface of the samples compared to the experiments performed at low values of the frontal gap.

By reducing the operating power of the ultrasonic chain with about 40%, a roughness decrease of the frontal surface of the samples is obtained.

Based on the analysis of the model achieved using finite element method concerning ultrasonic removal mechanism, it was found that:

In ultrasonic processing, the high values of the frontal gap require very high ultrasonic power to reduce the roughness, the ultrasonic shock waves propagating in a direction perpendicular to the sample surface.

At ultrasonic processing, a reduced frontal gap allows the use of much lower values of ultrasonic pressure, the ultrasonic shock waves being directed parallel to the processed surface, resulting reduced roughness.

Future researches will be focused on:

The extension of the studies will approach lower values of the gap between the end of ultrasonic chain and the surface of the samples, as well as wider range of the variation of the power applied on the ultrasonic chain in order to optimize the process.

The hybrid technology, anodic dissolution in the ultrasonic field, will be applied in order to obtain a higher quality of the surface processed by the synergy created by the combination of the electrochemistry and the ultrasounds.

## REFERENCES


1. *** Titanium Grade Overview, available at: http://www.supraalloys.com/titanium-grades.php, accessed at: 4.01.2019.
2. *** TiAl6V4 Titanium Alloy, available at: http://www.arcam.com/wp-content/uploads/Arcam-Ti6Al4V-Titanium-Alloy.pdf, accessed at:4.01.2019.
3. Inagaki I., Takechi T., Shirai Y., Ariyasu N., *Application and Features of Titanium for the Aerospace Industry*, Nippon steel & Sumitomo metal technical report no. 106, 2014, available at: http://www.nssmc.com/en/tech/report/nssmc/pdf/106-05.pdf, accessed at: 4.01.2019.
4. *** Titanium TI-6AL-4V Properties & Common Uses, 2016, available at: https://titaniumprocessingcenter.com/titanium-ti-6al-4v-properties-common-uses/, accessed at: 4.01.2019.
5. *** Titanium Ti-6Al-4V (Grade 5), Annealed available at: http://asm.matweb.com/search/SpecificMaterial.asp?bassnum=mtp641, accessed at: 4.01.2019.
6. *** Titanium Alloys - Ti6Al4V Grade 5, available at: https://www.azom.com/properties.aspx?ArticleID=1547, accessed at: 4.01.2019.
7. Soare, O., Lepădatu, D., Vălu, T., Dobre, D., *The Influence of ultrasonic field on the behavior of corrsosion of Ti alloyes in sea environment (in Romanian),* Scientific Session – Polytechnic University of Bucharest, (2018).
8. Ghiculescu, D., *Computer aided engineering and machining of nonconventional processes (in Romanian),* Printech, Bucharest, (2013).
9. Drobotă, V., *Materials resistance (in Romanian),* Didactic and Pedagogical, Bucharest, (1983).